INTERFACE

royalsocietypublishing.org/journal/rsif

Report

Cite this article: Reznikov K, Melnikov V, Sapir N. 2025 Estimating large birds' radar cross-section for aeroecology studies using T-matrix modelling. *J. R. Soc. Interface* **22**: 20250510.
https://doi.org/10.1098/rsif.2025.0510

Received: 3 June 2025
Accepted: 22 August 2025

Subject Category:
Life Sciences–Earth Science interface

Subject Areas:
environmental science, biometeorology, biophysics

Keywords:
avian migration, electromagnetic modelling, radar aeroecology, radar cross-section, soaring birds

Author for correspondence:
Korin Reznikov
e-mail: korin.reznikov@gmail.com

Electronic supplementary material is available online at https://doi.org/10.6084/m9.figshare.c.8044373.

THE ROYAL SOCIETY
PUBLISHING

Estimating large birds' radar cross-section for aeroecology studies using T-matrix modelling

Korin Reznikov[1], Valery Melnikov[2] and Nir Sapir[1]

[1]Department of Evolutionary and Environmental Biology and Institute of Evolution, University of Haifa, Haifa, Israel
[2]Cooperative Institute for Severe and High-Impact Weather Research and Operations (CIWRO), and NOAA/OAR National Severe Storms Laboratory, Norman, OK, USA

KR, 0009-0004-9131-3658; NS, 0000-0002-2477-0515

Radar technology has become a powerful tool for studying animal aeroecology in the lower atmosphere, particularly bird migration across large spatio-temporal scales. Quantifying bird density from radar data requires radar cross-section (RCS) estimates. Although RCS data exist for small bird species, large birds, especially soaring and flocking species, remain poorly characterized, partly due to technical challenges in measuring and modelling their complex morphology. This study introduces a practical and accessible modelling framework for estimating species-specific RCS in large birds, using the T-matrix electromagnetic scattering method, based on geometrically simplified representations of bird morphology. We computed spherical RCS values for 11 large bird species across C- and S-band radar wavelengths and compared them with both spherical and prolate spheroidal RCS estimates obtained using the WIPL-D software, a method previously validated for biological targets. As expected, the spherical simplification led to a systematic overestimation of RCS relative to a more anatomically representative model. However, the bias was consistent and can be corrected using regression-derived scaling factors. This approach addresses the critical lack of empirical RCS data for large birds, offering an alternative that can be implemented in open-source platforms. It can be integrated with automated detection tools to enhance our understanding of migration patterns in understudied bird groups and to support efforts to mitigate bird–aircraft collisions.

1. Introduction

Radar is a fundamental tool for studying animal aeroecology in the lower atmosphere [1,2]. Over recent decades, advancements in radar aeroecology have enabled large-scale, non-invasive monitoring of aerial wildlife, revealing spatio-temporal migration patterns [3,4], environmental effects on aerial bioflow [5–8] and contributing to the reduction of bird–aircraft collisions and other human–wildlife conflicts [9–11].

An essential component for estimating aerial biomass and bird density from radar reflectivity is the bird's radar cross-section (RCS hereafter) [12–16]. This parameter plays a central role in converting radar reflectivity (dBZ) into biologically meaningful quantities such as bird density [13,14,17]. As described in the standard radar equation [18] and demonstrated in biological applications by Dokter *et al.* [14], this conversion depends on the radar wavelength and the refractive index of the target. The term RCS refers to a property of a target that quantifies the amount of electromagnetic energy scattered from the target in all directions. It is computed based on the backscatter cross-section (BCS hereafter), which differs from RCS by quantifying only the electromagnetic energy scattered directly back towards the radar, resulting in a smaller value by a factor of 4π (equations (2.1) and (2.2)) [19,20]. Both BCS and RCS depend on several factors, including the target's shape, its orientation relative to the incident radar beam, the refractive index of the target and the radar wavelength [16].

Early studies that estimated birds' RCS relied mainly on theoretical calculations and laboratory measurements, mostly of small to medium-sized bird species [16,21–26]. Over time, advanced modelling approaches have emerged, with the most widely used method introduced by Dokter *et al*. [14], giving a constant bird RCS of 11 cm², representing an average passerine [14]. Despite these developments, most data remain focused on small birds, leaving a critical gap in RCS information for larger birds, many of which are soaring species.

To address this gap, we applied two electromagnetic scattering models commonly used in radar science—the T-matrix and the WIPL-D methods—to estimate the RCS of large bird species across two radar wavelengths.

In electromagnetic scattering models, two main parameters that determine the calculated RCS are the target's geometry and the refractive index, as noted above. Both factors influence the magnitude of the scattered wave [16]. Due to the high water content in biological targets, it is commonly assumed that their refractive index is equivalent to that of water [16,27]. In these models, the RCS is derived from the amplitude scattering matrix, which describes how an incoming electromagnetic wave is scattered by a target. For single-polarization weather radars, the scattering matrix is represented by a 2 × 2 matrix with four elements, each corresponding to transmitted and received wave polarizations in the vertical and horizontal directions [18,28]. In practice, single-polarization weather radars typically operate with horizontally polarized waves, making the horizontally received component, denoted as S_{22} or S_{hh}, the standard element used for RCS estimation.

The WIPL-D is a computational electromagnetics software based on the method of moments, which is well-suited for simulating the scattering properties of complex three-dimensional structures [29]. The WIPL-D method was previously validated as a reliable model for avian biological targets using both anatomically detailed shapes and simplified ellipsoidal representations [30]. It was shown that in cases where the target's body is large relative to the radar wavelength—specifically, when the body length exceeds approximately four times the wavelength—anatomical details have little influence on the magnitude and morphology of the modelled RCS [30]. In such cases, an ellipsoidal approximation becomes appropriate and computationally efficient. This makes the method particularly suitable for modelling large bird species, where this size criterion is met. When biological targets are represented as a prolate spheroid, they are characterized by a major axis, corresponding to the body length, and by a minor axis, corresponding to the body width. The body length is measured excluding the head and tail, while the body width excludes the wings, reflecting the dimensions that contribute the most to the scattering properties [23,27,31] (figure 1).

The T-matrix method is one of the most powerful and widely used theoretical techniques for computing electromagnetic scattering by non-spherical particles based on Maxwell's equations [32,33], but it has never been tested for biological targets. The method was implemented in the Fortran code [34] that was later integrated within a code in the Python programming language, facilitating the automation of the scattering property calculations [35]. However, the T-matrix method is subject to several limitations. Target shapes are limited to spheroids and cylinders, and large objects with very high or low aspect ratios present convergence problems [34,35]. As large bird species often exceed the size, ratio and shape complexity that the method handles efficiently, we implemented a spherical approximation for the birds' bodies. While spheres offer a computationally efficient simplification, they may not fully capture the anisotropic geometry of bird bodies, which more closely resemble spheroids elongated along the head-to-tail axis. This distinction is relevant for estimating orientation-dependent scattering, which plays a key role in the variability of birds' RCS measurements [36]. However, prior work has shown that such variability may average out across large flocks [37], suggesting that the spherical model can serve as a practical approximation in some radar ornithology applications. Moreover, the spherical simplification, though biologically limited, has been previously used in radar ornithology, with studies modelling birds as spheres of equivalent volume based on their body mass [16,25,38–40]. Additionally, Eastwood [25] and Urmy & Warren [38] noted that modelling birds as spheres produced reasonable agreement with measured RCS values [25,38].

The primary objective of our study was to generate species-specific RCS estimates for large birds using a practical and accessible modelling approach—the T-matrix method. To evaluate the applicability of this method for estimating the RCS of large birds based on spherical approximations, we compared its outputs with those of WIPL-D, a reference method capable of simulating more anatomically representative prolate spheroids. We mainly focused on diurnal soaring migrants, which pose the greatest risk for bird–aircraft collisions due to their large body mass and tendency to migrate in flocks. Our analysis addressed two key questions: (i) how does the T-matrix output compare with that of the WIPL-D method when both model birds as spheres, and (ii) what is the expected bias introduced by modelling birds as spheres rather than ellipsoids?

To address these questions, we first computed the RCS of spherical objects with both models. This allowed us to evaluate the reliability and accuracy of the T-matrix output compared with the WIPL-D output under identical geometric assumptions, where both methods model spheres. Then we computed the RCS of 11 large bird species as spheres with the T-matrix method, and as prolate spheroids with the WIPL-D method, allowing us to quantify the bias introduced by the spherical approximation, and propose a scaling factor to convert spherical RCS values into ellipsoidal equivalents.

2. Material and methods

To estimate the RCS of large bird species, we applied two electromagnetic scattering models: the T-matrix and the WIPL-D. The T-matrix model was used as our main method, computing RCS values by modelling birds as spheres, while the WIPL-D model was employed to validate the T-matrix results and assess the impact of simplifying bird morphology to spheres rather than

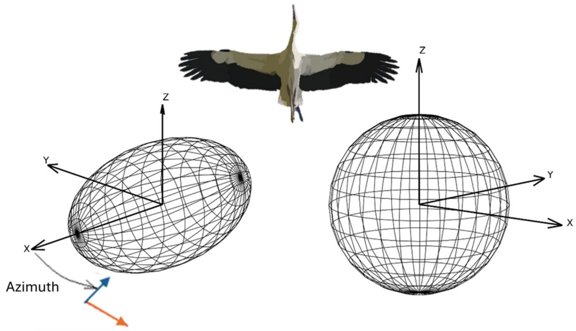

Figure 1. Scattering geometry of a white stork (illustration insert) modelled as a prolate spheroid (left) and as a sphere (right). The blue arrow indicates the direction of the incident electromagnetic wave, and the orange arrow shows its polarization.

prolate spheroids. Our analysis consisted of two evaluations: the first assessed the compatibility between T-matrix and WIPL-D outputs using spherical targets (spherical evaluation, hereafter), isolating potential effects of differences in the computational methods of the two models; the second evaluated the limitations of spherical modelling by comparing T-matrix simulations of spheres with WIPL-D simulations of prolate spheroids (hereafter sphere versus prolate evaluation), quantifying the error introduced by simplifying birds as spherical shapes.

2.1. Bird species and body size modelling

For the sphere versus prolate evaluation, we modelled 11 large bird species with body masses ranging from 168 to 6100 g, and major axis (i.e. bird's torso length) ranging from 12 to 34.8 cm: the black and white stork (*Ciconia nigra* and *Ciconia ciconia*), greater flamingo (*Phoenicopterus roseus*), European honey buzzard (*Pernis apivorus*), Eurasian (common) buzzard (*Buteo buteo*), black kite (*Milvus migrans*), Levant sparrowhawk (*Accipiter brevipes*), lesser spotted eagle (*Clanga pomarina*), steppe eagle (*Aquila nipalensis*), common crane (*Grus grus*) and white pelican (*Pelecanus onocrotalus*). These species are typical diurnal migrants, and some of them are considered dangerous to aerial transportation due to their high biomass and tendency to migrate in large flocks [9,41,42].

In conducting the sphere versus prolate evaluation, we calculated the birds' RCS by constructing two types of geometric representations of the birds. For the T-matrix method, birds were modelled as spheres with volumes equivalent to their actual body volumes (figure 1). To calculate the equivolume sphere for each species, we applied the standard mass–density equation, using the average body mass (in grams) of the focal bird species, based on Dunning [43], and assumed a body density equal to that of a water sphere, 1 g cm^{-3} [16,25]. Subsequently, the radius of the equivolume sphere was derived using the standard volume–radius equation for spheres. For the WIPL-D simulations, in addition to the equivolume sphere for each species, we generated three-dimensional models of birds as prolate spheroids, with the major axis representing torso length (excluding head and tail) and the minor axis corresponding to torso width (excluding wings; figure 1). To derive these dimensions for each species, we measured torso length and width dimensions from reference images showing birds viewed from directly below, with wings and legs fully extended [44]. Measurements were performed using the image analysis software Inkscape [45]. The measured axes were then divided by two to obtain the radius (semiaxes hereafter) used for the models (electronic supplementary material, table S1).

2.2. T-matrix modelling

For the T-matrix modelling, we used the PyTMatrix Python package to compute the scattering matrix [35]. The computation of the scattering matrix by the model requires defining several key parameters related to the target and radar system: (i) the axis ratio of the target, (ii) the radius of the target, (iii) the radar wavelength, (iv) the scattering direction, and (v) the complex refractive index denoted as m. Note that parameters (ii) and (iii) should be in the same units.

Accordingly, we constructed four models: two for the spherical evaluation, where we assessed the correspondence between T-matrix and WIPL-D outputs using spherical targets, and two for the sphere versus prolate evaluation, where we compared T-matrix spheres with WIPL-D prolate spheroids to quantify the bias introduced by shape simplification. Each pair of models was run at two typical radar wavelengths, C-band and S-band.

For all models, (i) we configured the axis ratio to one to represent spheres; (ii) for the first two spherical models, we used a range of spherical radii from 3 to 13 cm. For the second two sphere versus prolate models, we applied the calculated equivolume sphere radius (in cm) for each bird species; (iii) we set the radar wavelength to 5.3 cm for C-band simulations and 10 cm for S-band simulations; (iv) we used the default scattering direction of the model, 90° side view, noting that for spheres, the scattering matrix is independent of direction; and (v) we defined the complex refractive index as that of water at 40°C: for C-band, m = (8.45, 0.74); for S-band, m = (8.52, 0.43) [42].

From the computed scattering matrix, we extracted the element S_{22}, which represents horizontally polarized backscatter, and used it to calculate the BCS and RCS values using the following equations [46]:

$$\sigma_{BCS} = |S_{22}|^2, \tag{2.1}$$

$$\sigma_{\mathrm{RCS}} = 4\pi\sigma_{\mathrm{BCS}}, \tag{2.2}$$

where σ_{BCS} denotes the BCS, S_{22} denotes the scattering matrix element with horizontally polarized backscatter and σ_{RCS} indicates the RCS.

2.3. WIPL-D modelling

We employed the WIPL-D Pro electromagnetic simulation software to compute RCSs. Following the approach used in the T-matrix analysis, we constructed four models—two spherical models for the spherical evaluation and two prolate spheroidal models for the sphere versus prolate evaluation, where each pair of models was simulated at both C-band and S-band radar wavelengths. All simulations were conducted using horizontally polarized waves.

To generate the three-dimensional objects for the models, we specified five essential parameters for all four models: (i) axis ratio: for the spherical evaluation, we configured the axis ratio to one; for the sphere versus prolate evaluation, we calculated species-specific axis ratios by dividing the major semiaxis by the minor semiaxis (electronic supplementary material, table S1). (ii) Radius: for the spherical evaluation, we used radii ranging from 3 to 13 cm, identical to the T-matrix simulations; for prolate spheroids in the sphere versus prolate evaluation, we used the major semiaxis lengths of each bird species as detailed in the electronic supplementary material, table S1. (iii) Radar wavelength: consistent with the T-matrix models, we set 5.3 cm for C-band and 10 cm for S-band. (iv) Scattering orientation: for the spherical evaluation, we set a single orientation due to isotropy; for the prolate spheroidal evaluation, we ran simulations across azimuth angles from 0° (wave impinging on the tip of the prolate spheroid) to 90° (wave impinging on the side of the prolate spheroid). (v) Dielectric constant: we derived the dielectric constants from the complex refractive indices used in the T-matrix modelling, as the two properties are directly related. For C-band $\varepsilon = 70.85–12.57i$; for S-band $\varepsilon = 72.41–7.29i$, representing water properties at 40°C.

2.4. Statistical analysis

In the spherical evaluation, we assessed compatibility between the T-matrix and WIPL-D outputs using identical spherical targets. To quantify any differences between these two computational methods, we calculated the mean absolute error (MAE). This metric gives the same weight to all errors and enables the precise evaluation of minor discrepancies between the model outputs [47].

In the sphere versus prolate evaluation, we examined the potential bias introduced by approximating bird bodies as spheres. We compared RCS values calculated using the T-matrix method, where birds were modelled as equivolume spheres, with RCS values computed using WIPL-D, where birds were modelled as prolate spheroids. Because WIPL-D simulations produced RCS values across a wide range of azimuth angles, we first calculated species-specific mean RCS by averaging these values across all simulated orientations, following prior studies [29]. To quantify the error introduced by the spherical geometric simplification, we computed the MAE between the T-matrix spherical estimates and the WIPL-D spheroidal values. This provided a direct measure of the average deviation due to the spherical assumption. Additionally, we applied non-intercept linear regression analyses, appropriate for comparing interdependent variables [48]. The regression analysis enables us to characterize the spherical model in relation to the prolate spheroidal model and quantify the proportional bias introduced by the spherical approximation based on the regression equations. Furthermore, the resulting equations provided a corrective factor for converting spherical RCS estimates to prolate spheroid RCS values.

Both evaluations were analysed separately for the two radar bands (C-band and S-band). All statistical computations were performed using Python with the sklearn and SciPy modules.

3. Results and discussion

3.1. Spherical evaluation

The comparison between the T-matrix and WIPL-D outputs for spherical targets showed high similarity in RCS estimates across the full range of radii for both C-band and S-band wavelengths (3–13 cm; figure 2). For the C-band simulations, the MAE was 0.72 cm², with a mean percentage difference of 0.67%. The largest absolute difference was observed at a radius of 12.20 cm, where the WIPL-D estimated an RCS of 297.00 cm² and the T-matrix estimated 294.69 cm², a difference of 0.78%. For the S-band simulations, the MAE was 0.93 cm², with a mean percentage difference of 0.62%. The largest absolute deviation was 3.62 cm² at a radius of 11.70 cm, where the WIPL-D estimated an RCS of 272.98 cm² and the T-matrix estimated 269.36 cm², corresponding to a 1.33% difference.

The low MAE and percentage differences suggest that deviations introduced by methodological differences between the models are minimal across the two frequency bands. The high similarity in the RCS outputs shows that the T-matrix and WIPL-D models yield nearly equivalent RCS estimates for spherical targets, with no substantial bias or variability, despite differing computational frameworks.

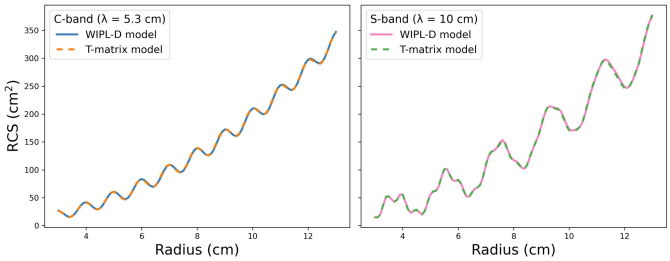

Figure 2. RCS estimates (*Y*-axis) of spherical targets modelled using the T-matrix and the WIPL-D methods across a range of 3—13 cm radii (*X*-axis), under two radar wavelengths, C-band (left panel) and S-band (right panel). Dashed lines present the results by the T-matrix model (left panel, orange; right panel, green), and the solid lines show the results by the WIPL-D model (left panel, blue; right panel, pink).

3.2. Spheres versus prolate evaluation

After confirming that methodological differences between the T-matrix and WIPL-D models do not contribute to substantial variation in RCS values, we proceeded to evaluate the effect of spherical geometric simplification on RCS estimation. In this second evaluation, we compared RCS values of 11 large bird species modelled as spheres using the T-matrix method to corresponding prolate spheroid representations modelled using the WIPL-D method (figure 3 and table 1).

For the C-band simulation, the RCS values calculated using the T-matrix method ranged from 15 cm² for the Levant sparrowhawk to 292 cm² for the white pelican, while the WIPL-D estimates for the same species ranged from 16 to 214 cm². The MAE between the two models was 39.80 cm², reflecting the average deviation introduced by the spherical simplification. The largest percentage difference was observed for the black kite, with a 61.43% discrepancy (WIPL-D: 46.13 cm²; T-matrix: 74.47 cm²), while the smallest difference of 5.62% occurred for the Levant sparrowhawk (table 1). A strong linear relationship was found between the two model outputs ($R^2 = 0.997$, $p < 0.001$; figure 3), expressed by the regression equation (3.1),

$$\mathrm{RCS}_{\mathrm{WC}} = 0.70\,\mathrm{RCS}_{\mathrm{TC}}, \tag{3.1}$$

where $\mathrm{RCS}_{\mathrm{WC}}$ and $\mathrm{RCS}_{\mathrm{TC}}$ denote the WIPL-D and T-matrix RCS, respectively, both for C-band radars, and the 0.70 value represents the regression coefficient.

For the S-band simulation, the T-matrix RCS estimates ranged from 53 to 260 cm², while the WIPL-D estimates ranged from 27 to 244 cm² for the same species as in the C-band simulation (table 1). The MAE was 36.98 cm². The largest percentage difference was found for the Levant sparrowhawk (96.75%), and the smallest was for the white pelican (6.46%). The results of the regression analysis showed a strong linear relationship ($R^2 = 0.979$, $p < 0.001$), described by equation (3.2),

$$\mathrm{RCS}_{\mathrm{WS}} = 0.78\,\mathrm{RCS}_{\mathrm{TS}}, \tag{3.2}$$

where $\mathrm{RCS}_{\mathrm{WS}}$ denotes the WIPL-D RCS, $\mathrm{RCS}_{\mathrm{TS}}$ denotes the T-matrix RCS, both for S-band radars, and 0.78 is the regression coefficient.

As anticipated, given the spherical simplification, the findings from the sphere versus prolate evaluation demonstrate that modelling bird bodies as spheres leads to an overestimation of RCS compared with prolate spheroid models. However, the spherical simplification introduces a consistent and predictable bias rather than random error, which can be effectively corrected using the regression equations provided (equations (3.1) and (3.2)). Importantly, the biases are attributable solely to shape assumptions, as the spherical evaluation confirmed that methodological differences between the T-matrix and WIPL-D models are negligible.

In light of the limited availability of empirical RCS data for large birds, this approach also helps address a persistent knowledge gap in radar aeroecology. Most available measurements focus on small species and are typically obtained under laboratory conditions using X-, L- or S-band radars, a set-up impractical for larger species [16,21–25,49]. As a result, empirical RCS values for large, flocking birds such as raptors and storks remain extremely limited. The few available references include field-based X-band measurements of geese flocks (1000–10 000 cm²) [22] and generalized S-band observations of unidentified flocks (approx. 10 000 cm²) [16], both of which reflect flock-level rather than species-specific estimates, without reporting flock sizes. A more directly comparable estimate is reported by Horton *et al*. [40], who used a body-mass regression model to estimate a spherical RCS of approximately 80 cm² for a 583 g bird. Consistent with this, our S-band simulations for a common buzzard (690 g) yielded a spherical RCS of 99 cm². In contrast, the Federal Aviation Administration's 'Standard Avian Target' assigns a value of 250 cm² to a 500 g bird, but lacks information on species identity or radar characteristics and probably overestimates RCS [26]. To our knowledge, no other species-specific RCS data are available for large flocking birds, further highlighting the value of simulation-based methods for filling this critical gap.

Our study highlights the practical value of the T-matrix method as a tool for estimating species-specific RCS in large birds. It is computationally efficient, implemented in open-source Python libraries, and can be easily integrated into automated processing pipelines. Nonetheless, certain limitations should be considered when interpreting RCS values derived from simplified geometries. In the absence of anatomically detailed models, prolate spheroids serve as a useful approximation of avian body shape. However, their accuracy decreases when the bird's body length is less than approximately four times the radar wavelength for anatomical versus ellipsoidal models [30]. Under such conditions, particularly for smaller birds in S-band radar simulations, where the wavelength is longer, anatomical details may still influence scattering behaviour and affect the precision of both the WIPL-D RCS values and the correction factor derived from them. To additionally examine the influence of

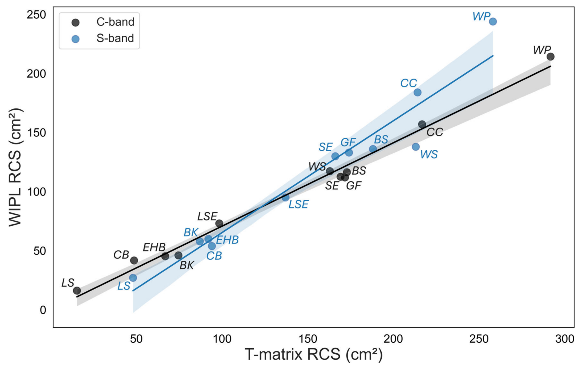

Figure 3. RCS values (cm^2) calculated using the T-matrix method (*X*-axis) compared with RCS values (cm^2) obtained from the WIPL-D method (*Y*-axis). The data represent 11 large bird species, modelled as spheres in the T-matrix method and as prolate spheroids in the WIPL-D method, with calculations performed for C-band (black) and S-band (blue) radars. The bird species names are written as abbreviations: BS, black stork; WS, white stork; GF, greater flamingo; EHB, European honey buzzard; BK, black kite; LS, Levant sparrowhawk; CB, common buzzard; LSE, lesser spotted eagle; SE, steppe eagle; CC, common crane; WP, white pelican. The dots represent the calculated RCS, and the regression line shows the model fit with a CI of 95%, shown by the shaded area (C-band regression equation: $RCS_{WC} = 0.7 \times RCS_{TC}$, $p < 0.001$, $R^2 = 0.997$; S-band regression equation: $RCS_{WS} = 0.78 \times RCS_{TS}$, $p < 0.001$, $R^2 = 0.979$).

Table 1. Calculated RCS values (cm^2) for 11 large bird species, using the T-matrix method and the WIPL-D software for C- and S-band radars. The RCS values were computed for birds in a sphere shape for the T-matrix method while considering body mass. The body mass is the female–male average body mass, derived from Dunning [43].

common name	scientific name	mass (g)	WIPL-D RCS (cm^2) C/S band	T-matrix RCS (cm^2) C/S band
black stork	*Ciconia nigra*	3100	116/136	173/188
white stork	*Ciconia ciconia*	3350	117/138	163/213
greater flamingo	*Phoenicopterus roseus*	3000	112/133	172/170
European honey buzzard	*Pernis apivorus*	780	45/60	67/89
black kite	*Milvus migrans*	815	46/58	74/81
Levant sparrowhawk	*Accipiter brevipes*	168	16/27	15/53
common buzzard	*Buteo buteo*	690	42/54	49/99
lesser spotted eagle	*Clanga pomarina*	1607	73/95	98/134
steppe eagle	*Aquila nipalensis*	2950	113/130	169/162
common crane	*Grus grus*	5050	157/184	217/215
white pelican	*Pelecanus onocrotalus*	7750	214/244	292/260

body size on model bias, we analysed the relationship between body length and percentage bias between the models using a Pearson correlation. The results for the S-band model showed a strong negative relationship ($r = -0.79$, $p = 0.003$). Smaller-bodied species, such as the Levant sparrowhawk and common buzzard, exhibited the largest relative differences between spherical and prolate spheroid models (96.3 and 83.3%, respectively; electronic supplementary material, table S2), whereas the largest species, including the white pelican and common crane, showed much smaller biases (6.6 and 16.8%, respectively; electronic supplementary material, table S2). In C-band, where most species fall within the four-wavelength threshold, no significant relationship between body length and model bias was found ($p = 0.2$). These results reinforce the notion that spherical simplifications may be less appropriate for smaller birds, particularly at longer wavelengths, highlighting the importance of considering size–wavelength ratios when using simplified geometries for RCS estimation.

In addition, the spherical T-matrix model does not account for orientation-dependent scattering, which can be significant for isolated individuals [27]. However, its utility increases in applications involving large flocks, where variation in orientation tends to average out [37]. This is especially important for flocking and soaring migrant species that are understudied in radar ecology, yet pose a disproportionately high risk for bird–aircraft collisions. The consequences of these collisions can result in billions of euros annually, in damaged aircraft, and most importantly, in the loss of human lives [9,10,42].

Our findings provide a flexible modelling framework that extends current radar aeroecological capabilities, particularly for large bird species lacking empirical RCS measurements. The accessibility and adaptability of the T-matrix method make it especially appealing for researchers seeking to estimate species-specific RCS without the complexity of high-fidelity electromagnetic models. By quantifying the limitations of spherical simplifications and proposing practical solutions, this study contributes to the development of applied radar aeroecology. Integrated with recent advances in automated detection algorithms [50], this modelling framework forms a foundation for estimating the density of migrating soaring bird flocks, using weather radars across large spatial and temporal scales, while supporting both ecological monitoring and bird–aircraft collision mitigation.

Further work is recommended to improve RCS accuracy for medium-sized species whose body length to wavelength ratio falls below the threshold for prolate spheroidal approximation [29]. One potential direction is the construction of more anatomically detailed three-dimensional models using WIPL-D, from which new correction factors can be derived and applied across a wider range of medium-sized birds. Such developments would expand the scope and precision of simulation-based RCS estimation and help close remaining gaps in the representation of avian targets in radar systems. Furthermore, since anatomical details also become negligible when modelling targets smaller than one quarter of a radar wavelength [30], the modelling strategy proposed here may also be useful for estimating insect RCS and should be further investigated.

Ethics. This work did not require ethical approval from a human subject or animal welfare committee.

Data accessibility. Data used in this study are available in the Supplementary Material file. The code and example dataset are archived on Zenodo [51].

Supplementary material is available online [52].

Declaration of AI use. We have not used AI-assisted technologies in creating this article.

Authors' contributions. K.R.: conceptualization, formal analysis, methodology, visualization, writing—original draft; V.M.: formal analysis, methodology, visualization, writing—review and editing; N.S.: funding acquisition, supervision, writing—review and editing.

All authors gave final approval for publication and agreed to be held accountable for the work performed therein.

Conflict of interests. We declare we have no competing interests.

Funding. Korin Reznikov's fellowship was provided by the Bloom Graduate School, University of Haifa.

References

1. Kelly JF, Stepanian PM. 2020 Radar aeroecology. *Remote Sens*. **12**, 1768. (doi:10.3390/rs12111768)
2. Bauer S *et al*. 2019 The grand challenges of migration ecology that radar aeroecology can help answer. *Ecography* **42**, 861–875. (doi:10.1111/ecog.04083)
3. Werber Y, Sextin H, Yovel Y, Sapir N. 2023 BATScan: a radar classification tool reveals large-scale bat migration patterns. *Methods Ecol. Evol*. **14**, 1764–1779. (doi:10.1111/2041-210x.14125)
4. Hu G, Lim KS, Horvitz N, Clark SJ, Reynolds DR, Sapir N, Chapman JW. 2016 Mass seasonal bioflows of high-flying insect migrants. *Science* **354**, 1584–1587. (doi:10.1126/science.aah4379)
5. Van Doren BM, Horton KG. 2018 A continental system for forecasting bird migration. *Science* **361**, 1115–1118. (doi:10.1126/science.aat7526)
6. Schekler I, Levi Y, Sapir N. 2024 Contrasting seasonal responses to wind in migrating songbirds on a globally important flyway. Proc. R. Soc. B **291**, 20240875. (doi:10.1098/rspb.2024.0875)
7. Schekler I, Smolinsky JA, Troupin D, Buler JJ, Sapir N. 2022 Bird migration at the edge – geographic and anthropogenic factors but not habitat properties drive season-specific spatial stopover distributions near wide ecological barriers. *Front. Ecol. Evol*. **10**. (doi:10.3389/fevo.2022.822220)
8. Shamoun-Baranes J, Liechti F, Vansteelant WMG. 2017 Atmospheric conditions create freeways, detours and tailbacks for migrating birds. *J. Comp. Physiol*. **203**, 509–529. (doi:10.1007/s00359-017-1181-9)
9. Nilsson C, La Sorte FA, Dokter A, Horton K, Van Doren BM, Kolodzinski JJ, Shamoun-Baranes J, Farnsworth A. 2021 Bird strikes at commercial airports explained by citizen science and weather radar data. *J. Appl. Ecol*. **58**, 2029–2039. (doi:10.1111/1365-2664.13971)
10. van Gasteren H, Krijgsveld KL, Klauke N, Leshem Y, Metz IC, Skakuj M, Sorbi S, Schekler I, Shamoun-Baranes J. 2019 Aeroecology meets aviation safety: early warning systems in Europe and the Middle East prevent collisions between birds and aircraft. *Ecography* **42**, 899–911. (doi:10.1111/ecog.04125)
11. Ginati A, Coppola D, Garofalo G, Shamoun-Baranes J, Bouten W, van GH, Dekker A, Sorbi S. 2010 FlySafe: an early warning system to reduce risk of bird strikes. *Eur Sp. Agency* **144**, 46–55. http://www.esa.int/SPECIALS/ESA_Publications/SEMO6LIRPGG_0.html
12. Buler JJ, Diehl RH. 2009 Quantifying bird density during migratory stopover using weather surveillance radar. *IEEE Trans. Geosci. Remote Sens*. **47**, 2741–2751. (doi:10.1109/tgrs.2009.2014463)
13. Chilson PB, Frick WF, Stepanian PM, Shipley JR, Kunz TH, Kelly JF. 2012 Estimating animal densities in the aerosphere using weather radar: to Z or not to Z? *Ecosphere* **3**, 1–19. (doi:10.1890/es12-00027.1)
14. Dokter AM, Liechti F, Stark H, Delobbe L, Tabary P, Holleman I. 2011 Bird migration flight altitudes studied by a network of operational weather radars. *J. R. Soc. Interface* **8**, 30–43. (doi:10.1098/rsif.2010.0116)
15. Probert-Jones JR. 1962 The radar equation in meteorology. *Q. J. R. Meteorol. Soc* **88**, 485–495. (doi:10.1002/qj.49708837810)
16. Vaughn CR. 1985 Birds and insects as radar targets: a review. *Proc. IEEE* **73**, 205–227. (doi:10.1109/PROC.1985.13134)
17. Gauthreaux SA, Belser CG. 1998 Displays of bird movements on the WSR-88D: patterns and quantification. *Weather Forecast*. **13**, 453–464. (doi:10.1175/1520-0434(1998)013<0453:DOBMOT>2.0.CO;2)
18. Doviak RJ, Zrnić D. 1993 *Doppler radar and weather observations*, 2nd edn. San Diago, CA: Academic Press.
19. Ishimaru A. 1978 *Wave propagation and scattering in random media*. New York, NY: Academic Press.
20. Bohren CF, Huffman DR. 1983 *Absorption and scattering of light by small particles*. New York, NY: Wiley.
21. Barry C JR, Erdahl B, Harrist R, Miller R, Smith J, Barnes C. 1973 *Angel clutter and the ASR air traffic control radar*. AD-775258. Washington, DC, USA: U.S Department of Transportation, Federal Aviation Administration.
22. Nohara TJ, Beason RC, Weber P. 2011 Using radar cross-section to enhance situational awareness tools for airport avian radars. *Human–Wildlife Interact.* **5**, 210–217. (doi:10.26077/sgas-w455)
23. Blacksmith P, Mack RB. 1965 On measuring the radar cross sections of ducks and chickens. *Proc. IEEE* **53**, 1125–1125. (doi:10.1109/proc.1965.4117)
24. Gong J, Yan J, Li D, Chen R. 2020 Comparison of radar signatures based on flight morphology for large birds and small birds. *IET Radar Sonar Navig.* **14**, 1365–1369. (doi:10.1049/iet-rsn.2020.0064)

25. Eastwood E. 1967 *Radar ornithology*. London, UK: Methuen & Co. Ltd.
26. Federal Aviation Administration (FAA)2010 *Airport avian radar systems*. Washington, DC: U.S. Department of Transportation, Federal Aviation Administration.
27. Melnikov VM, Istok MJ, Westbrook JK. 2015 Asymmetric radar echo patterns from insects. *J. Atmos Ocean Technol.* **32**, 659–674. (doi:10.1175/JTECH-D-13-00247.1)
28. Sakurai JJ, Jim JN. 2017 *Modern quantum mechanics*, 2nd edn. Cambridge, UK: Cambridge University Press.
29. Fernandes C, Salema C, Silveirinha M. 2001 WIPL-D compared with theory and experiment. In *17th Applied Computational Electromagnetics Conf. (ACES)*, Monterey, CA, USA, pp. 277–284.
30. Mirkovic D, Stepanian PM, Kelly JF, Chilson PB. 2016 Electromagnetic model reliably predicts radar scattering characteristics of airborne organisms. *Sci. Rep.* **6**, 35637. (doi:10.1038/srep35637)
31. Edwards J, Houghton E. 1959 Radar echoing area polar diagrams of birds. *Nature New Biol.* **184**, 1059–1060.
32. Mishchenko MI, Videen G, Babenko VA, Khlebtsov NG, Wriedt T. 2004 T-matrix theory of electromagnetic scattering by partciles and its applications: a comprehensive reference database. J. Quant. Spectrosc. Radiat. Transf. **88**, 357–406. (doi:10.1016/j.jqsrt.2004.05.002)
33. Waterman PC. 1965 Matrix formulation of electromagnetic scattering. *Proc. IEEE* **53**, 805–812. (doi:10.1109/proc.1965.4058)
34. Mishchenko MI, Travis LD. 1998 Capabilities and limitations of a current FORTRAN implementation of the *T*-matrix method for randomly oriented, rotationally symmetric scatterers. J. Quant. Spectrosc. Radiat. Transf. **60**, 309–324. (doi:10.1016/S0022-4073(98)00008-9)
35. Leinonen J. 2014 High-level interface to *T*-matrix scattering calculations: architecture, capabilities and limitations. *Opt. Express* **22**, 1655. (doi:10.1364/oe.22.001655)
36. Melnikov VM, Lee RR, Langlieb NJ. 2012 Resonance effects within S-band in echoes from birds. *IEEE Geosci. Remote Sens. Lett*. **9**, 413–416. (doi:10.1109/lgrs.2011.2169933)
37. Stepanian PM, Horton KG, Melnikov VM, Zrnić DS, Gauthreaux SA. 2016 Dual-polarization radar products for biological applications. *Ecosphere* **7**, e01539. (doi:10.1002/ecs2.1539)
38. Urmy SS, Warren JD. 2017 Quantitative ornithology with a commercial marine radar: standard-target calibration, target detection and tracking, and measurement of echoes from individuals and flocks. *Methods Ecol. Evol*. **8**, 860–869. (doi:10.1111/2041-210x.12699)
39. Shaefer GW. 1968 Bird recognition by radar: a study in quantitative radar ornithology. In *The problem of birds as pests* (eds RK Murton, EN Wright), pp. 53–113. New York, NY, USA: Academic Press.
40. Horton KG, Van Doren BM, La Sorte FA, Cohen EB, Clipp HL, Buler JJ, Fink D, Kelly JF, Farnsworth A. 2019 Holding steady: little change in intensity or timing of bird migration over the Gulf of Mexico. *Glob. Chang. Biol*. **25**, 1106–1118. (doi:10.1111/gcb.14540)
41. Jeffery RF, Buschke FT. 2019 Urbanization around an airfield alters bird community composition, but not the hazard of bird–aircraft collision. *Environ. Conserv*. **46**, 124–131. (doi:10.1017/s0376892918000231)
42. Marra PP, Dove CJ, Dolbeer R, Dahlan NF, Heacker M, Whatton JF, Diggs NE, France C, Henkes GA. 2009 Migratory Canada geese cause crash of US Airways Flight 1549. *Front. Ecol. Environ*. **7**, 297–301. (doi:10.1890/090066)
43. Dunning Jr JB. 2008 Body masses of birds of the world. In *CRC handbook of avian body masses*, pp. 24–87, 2nd edn. Boca Raton, FL: CRC Press. (doi:10.1201/9781420064452)
44. Billerman SM, Keeney BK, Rodewald PG, Schulenberg TS. 2022 .*Birds of the world*. Ithaca, NY: Cornell Laboratory of Ornithology. See https://birdsoftheworld.org/bow/home
45. Mattingly WA, Kelley RR, Chariker JH, Weimken T, Ramirez J. 2015 An iterative workflow for creating biomedical visualizations using Inkscape and D3.js. *BMC Bioinform*. **16**, 10. (doi:10.1186/1471-2105-16-s15-p10)
46. Mishchenko MI. 2000 Calculation of the amplitude matrix for a nonspherical particle in a fixed orientation. *Appl. Opt*. **39**, 1026. (doi:10.1364/ao.39.001026)
47. Chai T, Draxler RR. 2014 Root mean square error (RMSE) or mean absolute error (MAE)? *Geosci. Model Dev.* **7**, 1247–1250. (doi:10.5194/gmdd-7-1525-2014)
48. Haryadi S. 2017 *The non-intercept linear regression method*. Bandung, Indonesia: Bandung Institute of Technology (Institut Teknologi Bandung). (doi:10.13140/RG.2.2.18721.71522)
49. Gauthreaux SA Jr, Shapiro A, Mayer D, Clark BL, Herricks EE. 2019 Detecting bird movements with L-band avian radar and S-band dual-polarization Doppler weather radar. *Remote Sens. Ecol. Conserv*. **5**, 237–246. (doi:10.1002/rse2.101)
50. Schekler I, Nave T, Shimshoni I, Sapir N. 2023 Automatic detection of migrating soaring bird flocks using weather radars by deep learning. *Methods Ecol. Evol*. **14**, 2084–2094. (doi:10.1111/2041-210x.14161)
51. KorinRez. 2025 KorinRez/RCS_T-matrix: First release (v1.0.0). Zenodo. (doi:10.5281/zenodo.16895220)
52. Reznikov K, Melnikov V, Sapir N. 2025 Supplementary material from: Estimating large-birds' radar cross section for aeroecology studies using T-matrix modeling. Figshare. (doi:10.6084/m9.figshare.c.8044373)